

# U(VI) ion adsorption thermodynamics and kinetics from aqueous solution onto raw sodium feldspar and acid-activated sodium feldspar

Dexin Ding · Pingkun Fu · Le Li · Xin Xin ·  
Nan Hu · Guangyue Li

Received: 25 October 2013 / Published online: 12 January 2014  
© Akadémiai Kiadó, Budapest, Hungary 2014

**Abstract** The raw sodium feldspar (RSF) is activated with the concentrated sulfuric acid solution and the acid activated sodium feldspar (AASF) is obtained. The results obtained from the mercury intrusion method show that the acidification can increase the porosity and the specific surface area. The effects of the initial pH, contact time and ambient temperature on the adsorption of U(VI) ions are investigated in a batch process. The adsorption efficiency amounts to the highest at pH 6 and the adsorption equilibrium is reached in 600 min. The pseudo-second-order model is found to be more suitable for the adsorption process than the pseudo-first-order model and intra-particle model, indicating that the chemical adsorption is the predominant step for the adsorption process. Langmuir model is found to describe the adsorption process better than Freundlich model. This proves that the main form of U(VI) ions attached to RSF and AASF is the monolayer coverage. The thermodynamic parameters prove that the adsorption process is a spontaneous endothermic one. It was also found that acid activated treatment can help increase the adsorption rate and capacity. The results show that RSF and AASF can be used as a novel low cost adsorbent for removal of U(VI) ions from the low concentration aqueous solution.

**Keywords** Sodium feldspar · U(VI) ion adsorption · Low concentration aqueous solution · Kinetic · Water treatment

## Introduction

U(VI) ions are the predominant toxic metal ions in the wastewaters produced by the uranium mining and hydrometallurgy. U(VI) ions can transport and accumulate into human body through the food chain and ultimately lead to radiation damage and even death [1]. The conventional techniques have been found to be economically inefficient and environmentally unfriendly when they are used for dealing with the wastewaters in low concentration of U(VI) ions [2, 3]. Therefore, efforts are turning to low-cost and high efficiency approaches to overcome these challenges. Breakthroughs have been made on using mineral materials as adsorbents for the removal of the U(VI) ions from aqueous solution. Natural sepiolite [4] and thermally activated bentonite [5] have been reported to have 96 and 66.2 % of the adsorption efficiency. Kaolin [6], diatomite [7] and attapulgite [8] have also been reported to have 76, 97 and 95 % of the adsorption efficiency. These materials have been found to have high specific surface areas and good adsorption properties [9].

However, the feldspar for the adsorption of heavy metals has not attracted enough attention even though it is a rich diagenetic mineral [10]. Albite has been found to have only 58 % adsorption efficiency for U(VI) ions [11]. The two possible binding modes between the feldspar and U(VI) ions have been proposed [12] and the diffusion of U(VI) ions on the feldspar surface has been found to be a preferential process [13]. Moreover, the minerals are cheap and abundant and do not substantially cause new pollution

---

D. Ding (✉) · P. Fu · X. Xin · N. Hu · G. Li  
Key Discipline Laboratory for National Defense for  
Biotechnology in Uranium Mining and Hydrometallurgy,  
University of South China, Hengyang 421001,  
People's Republic of China  
e-mail: yyyue0806@163.com; dingdxzz@163.com

L. Li  
School of Public Health, University of South China,  
Hengyang 421001, People's Republic of China

when used for the removal of U(VI) ions from aqueous solution.

Some researchers have found that the acidification treatment of these minerals can help improve their surface properties and increase their specific surface areas [14, 15]. Acidified clays have been used to remove U(VI) [6, 16], lead [17], chromium [18], Ni(II) [19] and Cu(II) [20] etc. The researchers believed that the acidification treatment would make  $H^+$  easily exchange with some cations in the crystal structure [17] and can contribute to producing the negative charge on the surface to enhance the adsorption capability for cations [21]. Nevertheless, few reports have focused on the modified sodium feldspar with inorganic acid and its application in the adsorption of U(VI) ions from low concentration aqueous solution. In the present work, the adsorption of U(VI) ions from low concentration aqueous solution by RSF and AASF was studied.

## Experimental

### Materials

#### Adsorbents

Raw sodium feldspar (RSF) powders for this study were purchased from Yuyuan Mineral Processing Company (China). The AASF was prepared using the method below. First, 10 g of the sample powders and 100 mL of the concentrated sulfuric acid solution were mixed in a 500 mL beaker. Then the beaker was kept being stirred and heated for 6 h on a magnetic stirring apparatus. Finally, the mixture was filtered and washed repeatedly with double-distilled water and then dried in oven for use.

#### Adsorption studies and calculation

RSF and AASF were used to adsorb U(VI) ions from aqueous solution in the shaker bath at a speed of 200 rpm. The initial concentration of the solution was set to  $0.5 \text{ mg L}^{-1}$  when the effects of the solution pH and contact time on the adsorption of U(VI) ions were investigated. The pH of the solutions was adjusted to the required value from 3 to 8. And 0.1 g adsorbent and 50 mL of uranium solution were added into a 150 mL Erlenmeyer flask and the flask was immediately put in the shaker and kept being shaken at  $30 \text{ }^\circ\text{C}$  for a period of time. When the equilibrium was investigated, the initial concentration of U(VI) ions was set to  $0.1\text{--}1 \text{ mg L}^{-1}$ . When the thermodynamic studies were conducted, the temperature for the shaker bath was set to  $15\text{--}45 \text{ }^\circ\text{C}$ . After each adsorption experiment was completed, the solution was centrifuged and the

concentration of U(VI) ions in the supernatant solution was determined by WGJ-III type trace uranium analyzer.

The pseudo-first-order model, pseudo-second-order model and intra-particle model were given below to estimate the adsorption kinetics of U(VI) ion onto RSF and AASF:

$$\log(q_e - q_t) = \log(q_e) - \frac{k_1 \cdot t}{2.3, 023}$$

$$\frac{t}{q_t} = \frac{1}{k_2 \cdot q_e^2} + \frac{1}{q_e} \cdot t$$

$$qt = ki \cdot t^{1/2}$$

where  $q_e$  and  $q_t$  are the adsorption capacities ( $\text{mg g}^{-1}$ ) of uranium at equilibrium and time  $t$ , respectively;  $k_1$  ( $\text{min}^{-1}$ ),  $k_2$  ( $\text{g mg}^{-1} \text{ min}^{-1}$ ) and  $k_i$  ( $\text{g mg}^{-1} \text{ min}^{-1/2}$ ) are the pseudo-first-order model, pseudo-second-order model and intra-particle model rate constants, respectively.

The Langmuir and Freundlich adsorption isotherms were used to model the experimental data.

$$\frac{1}{q_e} = \frac{1}{q_{\max}} + \left( \frac{1}{q_{\max} K_L} \right) \frac{1}{C_e}$$

$$\log q_e = \log K_F + \frac{1}{n} \log C_e$$

where  $q_{\max}$  is the maximum amount ( $\text{mg g}^{-1}$ ) of monolayer adsorption;  $K_L$  ( $\text{L mg}^{-1}$ ) is the Langmuir equilibrium constant;  $K_F$  ( $\text{mg g}^{-1}$ ) and  $n$  are the Freundlich constants indicating the capacity and intensity of adsorption, respectively.

The thermodynamic parameters including  $\Delta H^\circ$ ,  $\Delta G^\circ$  and  $\Delta S^\circ$  can be determined by fitting the experimental data from 288 to 318 K to the following equations:

$$\ln K_d = \frac{\Delta S^\circ}{R} - \frac{\Delta H^\circ}{R} \frac{1}{T}$$

$$\Delta G^\circ = \Delta H^\circ - T\Delta S^\circ$$

$$K_d = \frac{q_e}{C_e}$$

where  $\Delta H^\circ$  ( $\text{J mol}^{-1}$ ),  $\Delta S^\circ$  ( $\text{J K}^{-1} \text{ mol}^{-1}$ ) and  $\Delta G^\circ$  ( $\text{J mol}^{-1}$ ) are the enthalpy, entropy and Gibbs free energy, respectively;  $R$  ( $8.314 \text{ J mol}^{-1} \text{ K}^{-1}$ ) is the ideal gas constant and  $T$  (K) is the thermodynamic Kelvin temperature;  $K_d$  is the equilibrium distribution coefficient.

#### Selective adsorption studies

Taking into account the practical application of the adsorbent in wastewater, the selective adsorption of U(VI) ions by RSF and AASF was studied in a mixed solution comprising a plurality of metal ions ( $K^+$ ,  $Ca^{2+}$ ,  $Mg^{2+}$ ,  $Cu^{2+}$  and  $Pb^{2+}$ ), which they occur generally in most

effluents. The initial concentration of these metal ions is selected to be 5 mg L<sup>-1</sup> and the selective adsorption experiment was carried out under the optical conditions. The residual concentration of metal ions in the solution was detected by WYX-420 atomic absorption spectrophotometer. The following equations are used to calculate the U(VI) ions distribution coefficient (*D*) and selectivity adsorption coefficient (*K*):

$$D = \frac{(C_0 - C_e)V}{C_e W}$$

$$K_{U(VI)/M} = \frac{D_{U(VI)}}{D_M}$$

where *C*<sub>0</sub> and *C*<sub>e</sub> are the initial concentration and equilibrium concentration, (mg L<sup>-1</sup>); *V* and *W* are the solution volume and the adsorbent dosage, respectively; *D* (L g<sup>-1</sup>) represents the distribution ratio between the mass concentration of metal ion adsorbed onto the adsorbent and the residual mass concentration in the solution at equilibrium.

### Characterization of samples

The PoreMaster-60 mercury porosimetry analyzer with the pore size distribution range of 950–0.0036 μm from Quantachrome Instruments (America) was used to analyze the pores of the sample before and after acidification. The surface tension and the mercury contact angle were set to 480.0 mN m<sup>-1</sup> and 140.0°, respectively. The surface morphology was characterized using JSM-6360LV scanning electron microscope (SEM). Infrared absorption spectra of the samples were measured in the range 4,000–400 cm<sup>-1</sup> using IRPrestige-21 infrared spectrometer made in Japan with resolution of ±4 cm<sup>-1</sup> to get the information on functional groups.

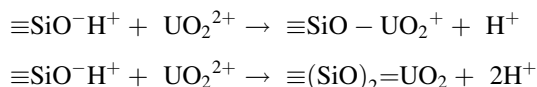
## Results and discussion

### Material characterization

The measured parameters for the pore structure of RSF and AASF are listed in Table 1. The results show that the acidification can increase the porosity and the specific surface area. This may be that some cations have been lost and other organic impurities have been carbonized, which

may help enhance the diffusion and transport of U(VI) ions from the aqueous solution to the interior of the sample [13].

The Fourier transform infrared (FT-IR) spectrometer was employed to analyze the groups in the AASF before and after adsorption. As shown in Fig. 1 the peaks at 3473.80 and 3238.48 cm<sup>-1</sup> represent the stretching vibration of O–H bond from the silanol groups (Si–OH) and water molecules (H–OH), respectively. And the bending vibration of O–H at 1639.49 and 1616.35 cm<sup>-1</sup> provides an evidence for the existence of water molecules in the crystal texture. The stretching vibration at 1598.99 cm<sup>-1</sup> is assigned to Si–O–Si groups. The two peaks at 775.38 and 727.16 cm<sup>-1</sup> are the characteristic peak spectra of quartz. The peaks at 644.22 and 428.2 cm<sup>-1</sup> are related to the stretching vibration and bending vibration of Al–O–Si groups, respectively. As shown in Fig. 1, the Si–O–Si and Al–O–Si groups have shifted from 644.22 to 622.88 cm<sup>-1</sup>, respectively. The O–H stretching vibration bands have shifted from 3473.80 and 3238.48 to 3469.94 and 3462.22 cm<sup>-1</sup>, respectively. It can be seen clearly from figure that the adsorption strength of hydroxyl groups has decreased greatly, indicating that the –OH group plays an important role in the formation of U–bond [22]. Thus, it is evident that the U(VI) adsorption onto AASF is likely to form the monodentate complexes or bidentate complexes as follows:



The SEM images of RSF (a) and AASF (b) samples are presented in Fig. 2. The figure shows that acid treatment makes the surface of the sample becomes loose and inflate. Many cracks appear on the surface and extend to the internal.

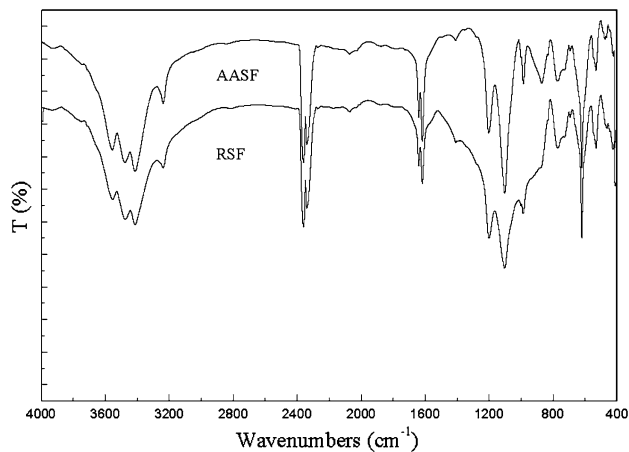
### Effect of initial pH

Figure 3 show the variation of the adsorption efficiency for U(VI) ions with the initial pH of the solution It can be seen that, as the pH increases from 3.0 to 6.0, the adsorption efficiency keeps on rise and that, when the pH increases from 6.0 to 8.0, the adsorption efficiency keeps on decrease. The adsorption efficiency of RSF and AASF for U(VI) ions reach the maximum at pH 6.0, Moreover, it was clearly found that the adsorption efficiency of AASF is greater than

**Table 1** Parameters for RSF and AASF from the mercury intruded method

	Specific surface area (m <sup>2</sup> g <sup>-1</sup> )	Throat (pore ratio)	Pore tortuosity	Permeability (m <sup>2</sup> )	Porosity (%)
RSF	1.3755	0.5974	1.7444	1.14–1.307 × 10 <sup>-18</sup>	42.97
AASF	2.0517	7.0814	1.6159	9.86–12.21 × 10 <sup>-16</sup>	55.34

that of RSF at the same pH condition, indicating that the acid activated treatment is conducive to increasing the adsorption of U(VI) ions from the aqueous solution. At the



**Fig. 1** FT-IR spectra of AASF before and after adsorption

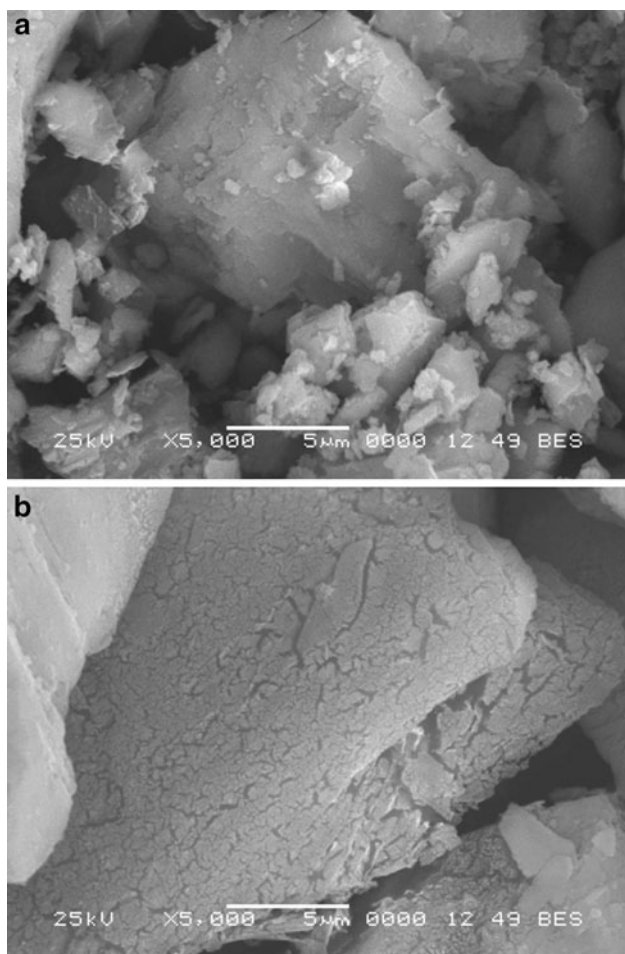


**Fig. 2** SEM images of RSF (a) and AASF (b)

low pH value, the molecular repulsion with  $\text{H}_3\text{O}^+$  ions having occupied some free sites prevents the  $\text{UO}_2^{2+}$  ions from approaching the sites. With the increase of pH,  $\text{UO}_2^{2+}$  ions also begin to hydrolyze [23] and form a variety of complexes [7, 24], including  $\text{UO}_2(\text{OH})^+$ ,  $(\text{UO}_2)_2(\text{OH})^{2+}$ ,  $(\text{UO}_2)_3(\text{OH})_5^+$ ,  $\text{UO}_2\text{CO}_3$ , and  $\text{UO}_2(\text{CO}_3)_3^{4-}$  etc. These species can be adsorbed according to the surface complexation theory [25, 26]. However, the electrostatic force and ion-exchange actions between those neutral and negatively charged species and the two adsorbents will reduce. As a result, the most suitable initial pH for the solution is 6.0.

#### Adsorption kinetics

Figure 4 shows the variation of the adsorption capacity with contact time onto raw sodium feldspar and acid

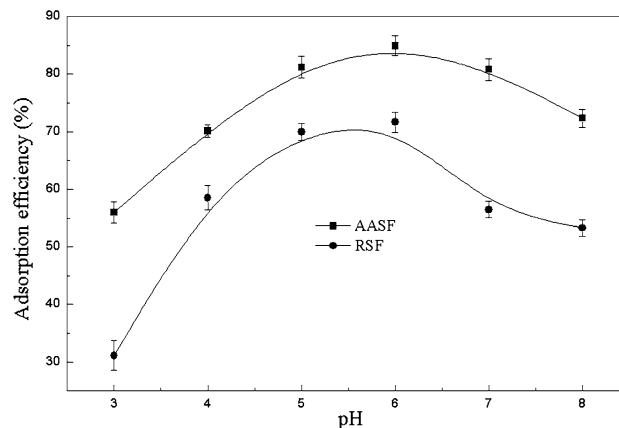


**Fig. 3** Effect of the initial pH value on the adsorption of U(VI) by RSF and AASF. Adsorbent dosage, 0.1 g; water sample volume, 50 mL; initial U(VI) concentration,  $0.5 \text{ mg L}^{-1}$ ; ambient temperature,  $30^\circ\text{C}$ ; contact time, 10 h

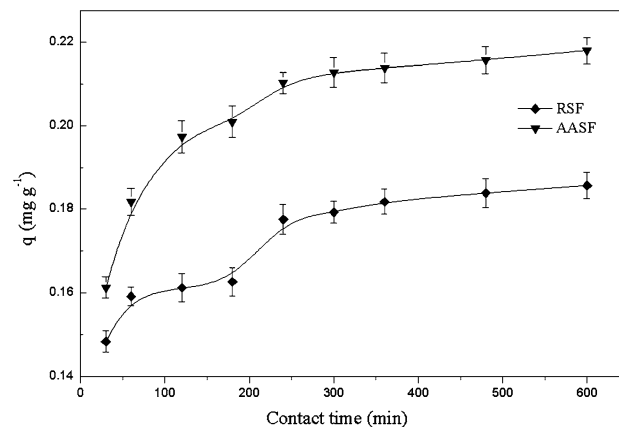


**Fig. 4** U(VI) adsorption kinetics onto RSF and AASF. Adsorbent dosage, 0.1 g; water sample volume, 50 mL; initial U(VI) concentration,  $0.5 \text{ mg L}^{-1}$ ; pH, 6.0; ambient temperature,  $30^\circ\text{C}$

**Table 2** Kinetics model constants for U(VI) adsorption onto RSF and AASF at 30 °C

	First-order kinetic model			Second-order kinetic model			Intra-particle diffusion model	
	$k_1$ (min <sup>-1</sup> )	$R^2$	$q_e$ (cal) (mg g <sup>-1</sup> )	$k_2$ (g mg <sup>-1</sup> min <sup>-1</sup> )	$R^2$	$q_e$ (cal) (mg g <sup>-1</sup> )	$k_i$ (mg g <sup>-1</sup> min <sup>-0.5</sup> )	$R^2$
RSF	0.0013	0.816	0.085	0.332	0.998	0.189	0.0025	0.843
AASF	0.0028	0.840	0.052	0.309	0.994	0.223	0.003	0.818

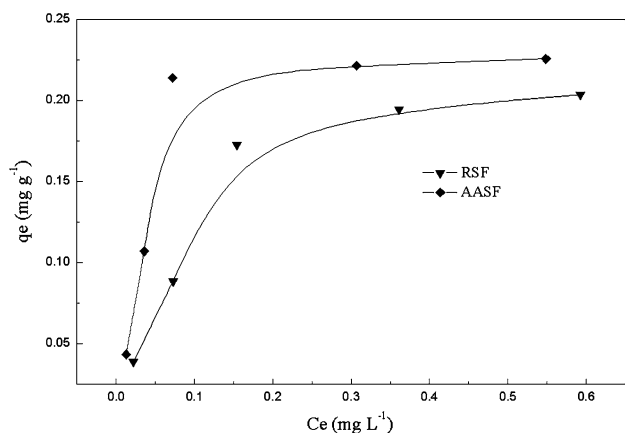


**Fig. 5** U(VI) adsorption isotherms onto RSF and AASF. Adsorbent dosage, 0.1 g; water sample volume, 50 mL; pH, 6.0; ambient temperature, 30 °C; contact time, 10 h

activated sodium feldspar. A comparison of the two curves indicates that AASF sample exhibit faster adsorption rate and larger adsorption capacity than RSF sample, suggesting that acid activation process increase the diffusion channel and also increase the amount of the active sites. Whereas the mass transfer resistance is on the rise due to the increase of repulsion between adsorbate molecules and the decreases of the concentration gradient [27]. The related parameters of the pseudo-first-order model, pseudo-second-order model and intra-particle model are listed in Table 2. The fitting correlation coefficients show that pseudo-second-order kinetic model is more suitable for describing the adsorption process, suggesting that the chemical adsorption is the predominant step for the adsorption process [28].

Adsorption isotherm

Figure 5 shows the U(VI) ions adsorption isotherms onto RSF and AASF from the low concentration aqueous solution. The correlation coefficients for Langmuir and Freundlich isotherm models are listed in Table 3. The results demonstrate that Langmuir model can well delineate the U(VI) adsorption process by RSF and AASF because of the higher correlation coefficient, and that the adsorption of U(VI) ions onto RSF and AASF is probably the monolayer

**Table 3** Langmuir and Freundlich isotherm constants for U(VI) adsorption onto RSF and AASF at 30 °C

	Langmuir isotherm model			Freundlich isotherm model		
	$q_m$ (mg g <sup>-1</sup> )	$K_L$ (L mg <sup>-1</sup> )	$R^2$	$K_F$ (mg g <sup>-1</sup> )	$n$	$R^2$
RSF	0.314	7.52	0.991	0.104	1.992	0.795
AASF	0.346	11.418	0.972	0.369	2.544	0.784

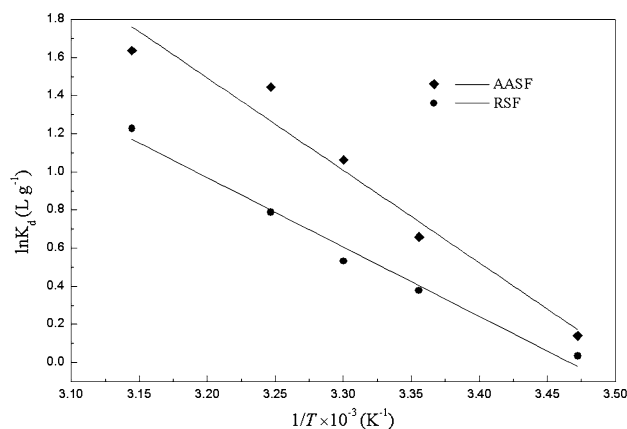


**Fig. 6** Effect of temperature on the thermodynamic parameters for the adsorption of U(VI) onto RSF and AASF

coverage. It also can be seen that the maximum amount of adsorption of U(VI) ions by AASF is greater than that by RSF, which indicates that acid treatment is contributed to enhancing the adsorption capacity of RSF.

Thermodynamic studies

The fitting curve of  $\ln K_d$  versus  $1/T$  is plotted in Fig. 6.  $\Delta H^\circ$  and  $\Delta S^\circ$  can be calculated from the slope and intercept of the curve, respectively. The calculated thermodynamic parameters for RSF and AASF are summarized in Table 4. It can be seen from the table that  $\Delta H^\circ$  is positive, indicating that the adsorption is endothermic process, that  $\Delta S^\circ$  is also positive, indicating that the adsorption reaction at the solid–liquid interface is an entropy-driven process and advantageous, and that  $\Delta G^\circ$  is negative, indicating that the adsorption of U(VI) ions by RSF and AASF process is a



**Table 4** Thermodynamic parameters for the adsorption of U(VI) onto RSF and AASF

	$\Delta H^\circ$ (kJ mol <sup>-1</sup> )	$\Delta S^\circ$ (kJ K <sup>-1</sup> mol <sup>-1</sup> )	$\Delta G^\circ$ (kJ mol <sup>-1</sup> )					$R^2$
			288 K	298 K	303 K	308 K	318 K	
RSF	30.17	0.11	-0.02	-1.06	-1.58	-2.11	-3.16	0.8799
AASF	40.29	0.14	-0.42	-1.83	-2.54	-3.24	-4.66	0.9471

**Table 5** Selective adsorption properties of the RSF and AASF

Cations	Distribution ratio (D, L g <sup>-1</sup> )		Selectivity coefficient ( $K_{U(VI)/M}$ )	
	RSF	AASF	RSF	AASF
UO <sub>2</sub> <sup>2+</sup>	0.61	1.88	1.0	1.0
K <sup>+</sup>	0.16	0.07	3.81	26.86
Ca <sup>2+</sup>	0.06	0.17	10.17	11.06
Mg <sup>2+</sup>	0.02	0.03	30.05	62.67
Cu <sup>2+</sup>	0.36	0.07	1.69	26.85
Pb <sup>2+</sup>	0.36	0.08	1.69	23.5

spontaneous one in the natural environment. Moreover, it is noticed that the value of  $\Delta G^\circ$  for AASF is less than that value for RSF at the same temperature, which indicates that acid activation favors to increase the degree of spontaneity.

#### Evaluation of the selective adsorption of U(VI) ions

The obtained results are shown in Table 5. It can be seen clearly that the distribution ratios of AASF for U(VI) ions was far greater than that of RSF, which means that acid activated treatment can help more U(VI) ions load on the adsorbent from the aqueous solution. Furthermore, the selectivity coefficient of RSF and AASF for U(VI) ions is greater than one and it is also found that the selectivity coefficient of AASF for each individual metal ion is far greater than that of RSF. Therefore, it is believed that RSF and AASF have a good selectivity for adsorption of U(VI) ions from a low concentration aqueous solution and the acid activated treatment is contributed to enhancing the selective adsorption of U(VI) ions.

#### Conclusions

The acidification treatment was found to enlarge the porosity and the specific surface area. Many groups were found to involve the adsorption but the -OH group was found to play a more significant role. The adsorption efficiency was found to depend on the initial pH of the solution and to reach the highest at pH = 6. The adsorption kinetics was found to be slow, taking 600 min to reach the equilibrium, the observed adsorption kinetics data, to agree with the pseudo-second-

order model, and the adsorption, to be dominated by chemical adsorption. Langmuir model was found to describe the adsorption process better than Freundlich model, indicating that the adsorbed uranium was in the form of monolayer coverage. The results also proved that AASF has faster adsorption rate and higher adsorption capacity than that of RSF. The adsorption was proved to be a spontaneous endothermic process. RSF and AASF performed a good selective adsorption of U(VI) ions from a low concentration aqueous solution and the acid activated treatment was found to be contributed to enhancing the selectivity.

**Acknowledgments** This research was supported by the National Natural Science Foundation of China (Grant Nos. 91326106, 11305087), the Scientific Research Foundation of Science and Technology Department of Hunan Province (Grant Nos. 2010GK2025, 2012SK3154), the Scientific Research Foundation of Education Department of Hunan Province (Grant No. 10A103).

#### References

- Guerra DL, Leidens VL, Viana RR, Airoidi C (2010) Amazon kaolinite functionalized with diethylenetriamine moieties for U(VI) removal: thermodynamic of cation–basic interactions. *J Hazard Mater* 180:683–692
- Rahman ROA, Ibrahim HA, Hung YT (2011) Liquid radioactive wastes treatment: a review. *Water* 3:551–568
- Li J, Zhang Y (2012) Remediation technology for the uranium contaminated environment: a review. *Procedia Environ Sci* 13:1609–1615
- Donat R (2009) The removal of uranium(VI) from aqueous solutions onto natural sepiolite. *J Chem Thermodyn* 41:829–835
- Aytas S, Yurtlu M, Donat R (2009) Adsorption characteristic of U(VI) ion onto thermally activated bentonite. *J Hazard Mater* 172:667–674
- Wang GH, Wang XG, Chai XJ, Liu JS, Deng NS (2010) Adsorption of uranium(VI) from aqueous solution on calcined and acid-activated kaolin. *Appl Clay Sci* 47:448–451
- Niu ZW, Fan QH, Wang WH, Xu JZ, Chen L, Wu WS (2009) Effect of pH, ionic strength and humic acid on the sorption of uranium(VI) to attapulgite. *Appl Radiat Isot* 67:1582–1590
- Aytas S, Akyil S, Aslani MAA, Aytekin U (1999) Removal of uranium from aqueous solutions by diatomite (Kieselguhr). *J Radioanal Nucl Chem* 240:973–976
- Ding Z, Frost R (2004) Study of copper adsorption on montmorillonites using thermal analysis methods. *J Colloid Inter Sci* 269:296–302
- Vidyadhar A, Rao KH, Forsberg KSE (2002) Adsorption of *N*-tallow-1,3-propanediamine-dioleate collector on albite and quartz minerals, and selective flotation of albite from Greek Stefania feldspar ore. *J Colloid Inter Sci* 248:19–29

11. Arnold T, Zorn T, Bernhard G, Nitsche H (1998) Sorption of uranium(VI) onto phyllite. *Chem Geol* 15:129–141
12. Walter M, Arnold T, Geipel G, Scheinost A, Bernhard G (2005) An EXAFS and TRLS investigation on uranium(VI) sorption to pristine and leached albite surfaces. *J Colloid Inter Sci* 282:293–305
13. Kerisit S, Liu CX (2012) Diffusion and adsorption of uranyl carbonate species in nanosized mineral fractures. *Environ Sci Technol* 46:1632–1640
14. Dékány I, Turi L, Fonseca A, Nagy JB (1999) The structure of acid treated sepiolites: small-angle X-ray scattering and multi MAS-NMR investigations. *Appl Clay Sci* 14:141–160
15. Rodriguez MAV, Gonzalez JDDL, Muñoz MAB (1994) Acid activation of a Spanish sepiolite: physicochemical characterisation, free silica content and surface area of products obtained. *Clay Miner* 29:361–367
16. Kilislioglu A, Aras G (2010) Adsorption of uranium from aqueous solution on heat and acid treated sepiolites. *Appl Radiat Isot* 68:2016–2019
17. Resmi G, Thampi SG, Chandrakaran S (2012) Removal of lead from wastewater by adsorption using acid-activated clay. *Environ Technol* 33:291–297
18. Arfaouia S, Frini-Srasra N, Srasra E (2008) Modelling of the adsorption of the chromium ion by modified clays. *Desalination* 222:474–481
19. Bhattacharyya KG, Gupta SS (2008) Influence of acid activation on adsorption of Ni(II) and Cu(II) on kaolinite and montmorillonite: kinetic and thermodynamic study. *Chem Eng J* 136:1–13
20. Bhattacharyya KG, Gupta SS (2011) Removal of Cu(II) by natural and acid-activated clays: an insight of adsorption isotherm, kinetic and thermodynamics. *Desalination* 272:66–75
21. Mukhopadhyay B, Walther JV (2001) Acid–base chemistry of albite surfaces in aqueous solutions at standard temperature and pressure. *Chem Geol* 174:415–443
22. Liu MX, Dong FQ, Yan XY, Zeng WM, Hou LY, Pang XF (2010) Biosorption of uranium by *saccharomyces cerevisiae* and surface interactions under culture conditions. *Bioresour Technol* 101:8573–8580
23. Sprynskyy M, Kowalkowski T, Tutub H, Cukrowska EM, Buszewski B (2011) Adsorption performance of talc for uranium removal from aqueous solution. *Chem Eng J* 171:1185–1193
24. Jang JH, Dempsey BA, Burgos WD (2006) Solubility of chelate: comparison and selection of complexation constants for U(VI). *Water Res* 40:2738–2746
25. Arnold T, Zorn T, Zänker H, Bernhard G, Nitsche H (2001) Sorption behavior of U(VI) on phyllite: experiments and modeling. *J Contam Hydrol* 47:219–231
26. Kowal-Fouchard A, Drot R, Simoni E (2004) Use of spectroscopic techniques for uranium(VI)/montmorillonite interaction modeling. *Environ Sci Technol* 38:1399–1407
27. Wang GH, Liu JS, Wang XG, Xie ZY, Deng NS (2009) Adsorption of uranium(VI) from aqueous solution onto cross-linked chitosan. *J Hazard Mater* 168:1053–1058
28. Pang C, Liu YH, Cao XH, Hua R, Wang CX, Li CQ (2010) Adsorptive removal of uranium from aqueous solution using chitosan-coated attapulgite. *J Radioanal Nucl Chem* 286:185–193